MODELING TEMPERATURE GRADIENTS NEAR LARGE VESSELS IN PERFUSED TISSUES

Michael C. Kolios, Michael D. Sherar, Arthur E. Worthington and John W. Hunt
Department of Medical Biophysics
University of Toronto
Toronto, Ontario
CANADA

Abstract

Vascular models model the effects of blood flow on temperature distributions during hyperthermia. These models explicitly analyze large vessel cooling for a limited number of vessels and use continuum models to predict average temperatures of perfused tissues. The analysis has traditionally been performed by assuming a constant Nusselt number to calculate heat transfer to thermally significant vessels. This assumption has a questionable validity during hyperthermia, especially for transient protocols. A vascular model is presented that does not require heat transfer coefficients to calculate heat transfer to/from thermally significant vessels; rather, the entire tissue/blood vessel domain is discretized and solved by finite differences. Results of modeling a large vessel embedded in perfused, heated tissue will be presented for two continuum models of microvascular heat transfer: the bioheat transfer equation (BHTE) and the effective thermal conductivity equation (ETCE). Furthermore, experimental data are presented that indicate the validity of model predictions and demonstrate the temperature gradients caused by large vessels in heated tissues in a *vitro* setting.

Nomenclature

c = specific heat capacity (J/kg/^{o}C)
dr = grid spacing in the radial direction (cm)
dz = grid spacing in the axial direction (cm)
k = thermal conductivity (W/cm/^{o}C)
k_{eff} = scalar effective conductivity of tissue (W/cm/^{o}C)

r, z = radial and axial coordinates (cm)
s = fraction of spacing dx for a non-uniform grid
u(r) = velocity of blood (cm/sec)
w = volumetric perfusion rate (g/cm^3/s)
P = volumetric power deposition rate (W/cm^3)
T = temperature (^{o}C)

α = best fit parameter equating perfusion and effective conductivity (g/cm^3/s)$^{-1}$
δ = blood vessel diameter (cm)
θ = angle in cylindrical coordinates (rad)
ρ = density (g/cm^3)
Δ = grid generation parameter

subscripts
art = arterial
b = blood
e = east node
i = node number
n = north node
s = south node
t = tissue
w = west node

Introduction

Prediction of temperature profiles for hyperthermia treatments is central to thermal dosimetry (Roemer 1990). The temperature information assists in the planning and assessment of treatments since therapeutic outcome is a function of temperature and exposure time. To

calculate temperature distributions during treatments models of tissue power absorption and cooling are required. For the latter, accurate formulations of bioheat transfer in perfused tissue are necessary. Vessels can be classified according to their convective strength: thermally significant and thermally insignificant. While the division is somewhat arbitrary (Baish 1992), it is necessary since all vessels in a heated filed cannot be modeled explicitly. The effects of the microvasculature are represented by a term that describes the collective effects of the smaller vessels of the circulation. The two prevalent models of microvascular heat transfer are the bioheat transfer equation (BHTE) and the effective thermal conductivity equation (ETCE). It is not clear which continuum model better describes microvascular heat transfer and limited data are available in the literature that compare the two models (Crezee *et al.* 1991; Moros *et al.* 1993a).

To estimate heat transfer to thermally significant vessels investigators have used constant heat transfer coefficients based on model problems such as the Graetz problem (Mooibroek and Langendijk 1991; Chen and Roemer 1992). The applicability of this approximation to hyperthermic situations is not clear. It implicitly assumes that the normalized vessel steady state radial temperature profiles are independent of axial position for thermally developing and developed blood, independent of perfusion of the surrounding tissues and of vessel shape. Furthermore, it implicitly assumes that the normalized radial temperature profiles are time invariant during tissue heating. There is evidence that the thermal entrance length for large vessels is a significant portion of the vessels length and that microvascular cooling, as modeled by an effective conductivity, can modify the heat transfer coefficient (Crezee and Lagendijk 1992). Moreover, vessel shape can modify heat transfer to vessels; elliptical channels of eccentricity ϵ=0.25 (that may be expected in the venous system) show differences in heat transfer coefficients of almost three orders of magnitude between the endpoints of the major and minor axes, albeit the differences average out when integrated over the circumference (Basmadjian 1990). Finally, since a major fraction of a hyperthermic treatment is in the tissue heating and cooling phases, a steady state cannot be assumed (Sapareto and Dewey 1984). Heat transfer to vessels for step changes in vessel wall temperature is greater until a steady state is achieved (Soliman and Chambre 1967). Therefore, a vascular model is required that can overcome these ambiguities. The model should produce accurate steady state and transient temperature data to predict thermal gradients near large vessels.

Methods

The solution domain is separated into two fields: the blood domain (consisting of the regions enclosed in large vessels) and the tissue domain (representing perfused tissue). The problem is solved for the vascular and tissue geometries in a fashion similar to the one proposed by Moros *et al.* (1993b). In this formulation, no prior assumptions are made about heat transfer to vessels; the conservation nature of the numerical methods implicitly model this. Therefore entrance region variations, the perfusion dependence of heat transfer coefficients and transient effects are included in the calculations.

The equations used to model heat transfer are solved numerically in cylindrical coordinates assuming a fully developed incompressible fluid with a parabolic velocity profile and θ symmetry:

$$\rho_b c_b \frac{\partial T}{\partial t} = k_b \left(\frac{\partial^2 T}{\partial^2 r} + \frac{1}{r} \frac{\partial T}{dr} + \frac{\partial^2 T}{\partial^2 z} \right)$$
$$-\rho_b c_b u(r) \frac{\partial T}{\partial z} + P_b \quad \text{blood region} \qquad (1)$$

$$\rho_t c_t \frac{\partial T}{\partial t} = k_{eff} \left(\frac{\partial^2 T}{\partial^2 r} + \frac{1}{r} \frac{\partial T}{dr} + \frac{\partial^2 T}{\partial^2 z} \right)$$
$$-w_b c_b (T(r,z) - T_{art}) + P_t \quad \text{tissue region} \qquad (2)$$

The vessel domains are modeled by equation 1 and the tissue regions by 2. Power absorption in the vessel and the tissues could be adjusted to model for ultrasound heating ($P_t \gg P_b$) or microwave heating ($P_t \sim P_b$). The cooling effects of the microcirculation can be modeled by the Pennes model by setting $k_{eff} = k_t$ in 2 and adjusting w_b to the appropriate value. Similarly, for the ETCE model w_b is set to zero and k_{eff} assigned the value of interest. Furthermore, the model allows simultaneous use of the continuum models, as proposed by Lagendijk *et al.* (1992).

The equations were solved by the method of finite differences. The conductive terms in the equation were discretized according to central difference formulations and the convective terms according to upwind differences (Patankar 1980). The resulting matrices were solved by using the alternate-direction implicit method (ADI), allowing modeling of steady-state and transient conditions (Croft and Lilley 1977). To handle conductivity discontinuities at the vessel-tissue interface for the ETCE model, the harmonic mean of the vessel and tissue conductivities was used at the vessel wall (Patankar 1980). This is necessary since the ratios of the conductivities k_{eff}/k_b at the vessel wall can be as high as 10 to 20. A variable grid was utilized to concentrate the grid points near the vessel by linearly increasing the radial step size from the
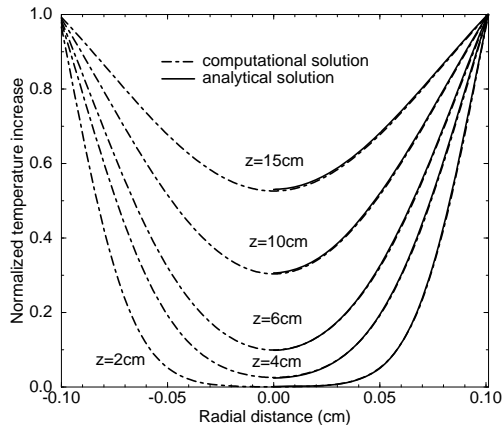
FIGURE 1: Comparison of analytical and computational solution for the Graetz problem with *plug* flow at different depths (<u>=10cm/s). Good agreement between numerical and analytic solution for 39 nodes radially.

FIGURE 2: Geometry of computer simulations. Three concentric cylinders represent the tissue volume (r= 4cm), heated region (r= 2cm) and the blood vessel (r= variable).

vessel center. A brief derivation of the finite difference equations is given in the appendix.

Results

The numerical results were compared to analytical solutions of simplified problems. To compare radial temperature profiles in the flow, the Graetz problem with plug flow was used as a benchmark (Shah and London 1978). The maximum deviation found was $\sim$ 2.0% for the range of parameters used in the simulations and the minimum amount of radial intravascular nodes (figure 1). To compare the tissue temperature predictions, a large velocity was assigned to the flow equivalent to setting the surface of the blood vessel to a constant temperature. The analytical and numerical solutions agreed for a range of power depositions and perfusion values (Kolios 1994).

Simulations were performed to assess how microvascular heat transfer modifies thermal gradients near large vessels in heated tissues. The parameters used are shown in table 1. Examples in this work are based on a δ=1.4mm blood vessel assigned an average blood velocity of 10cm/s. The simulation geometry is shown in figure 2. The vessel is located at the center of a cylinder, within a heated volume of radius 2 cm representing a hypothetical case of tissue heating. The radial boundaries are kept at body temperature and an adiabatic condition is implemented for both axial boundaries. Uniform power absorption is assumed throughout the entire field. Bioheat transfer in perfused tissues was modeled according to the BHTE or the ETCE. The system was allowed to reach a steady state and the temperatures were nor-
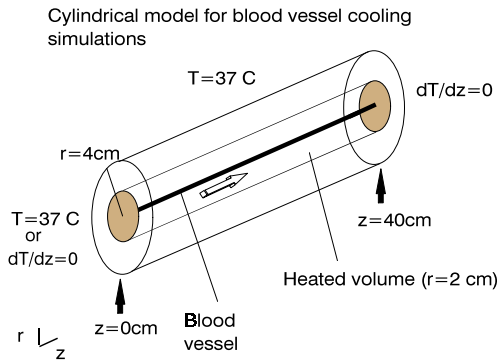
malized to the maximum temperature in the field to compare the data. Temperature gradients in the absence of perfusion dominate the heated field, extending well beyond the oxygen diffusion limit for the vessels. For vessels with $\delta \gg 0.1$ mm the effects persist for axial distances greater than the physical lengths of the vessels, and cool a significant portion of tissue. Nevertheless, vessel wall temperatures can be higher than the temperatures of the mixing-cup or center-line temperatures of the blood itself. Figure 3 illustrates the center-line, mixing cup, vessel wall and maximal tissue temperatures for a δ=1.4 mm diameter vessel, embedded in perfused tissue (w_b=0.008 g/cm^3/s, BHTE model). The radial gradients within the vessel allow the vessel wall temperature to be $\sim$ 10-20% higher than the center-line blood temperature. For vessels of diameter $\delta \leq 0.2$ mm, the temperature deviation within the vessel is insignificant. Increased perfusion of the surrounding tissue, according to the BHTE, results in more efficient blood heating and reduction of the radial and axial tissue temperature gradients. The thermal equilibration lengths (TEL) of the vessels, defined as the distance required for the blood to reach 63% of the surrounding tissue temperature, re-

TABLE 1: Listing of physical parameters used in simulations (Duck 1990)

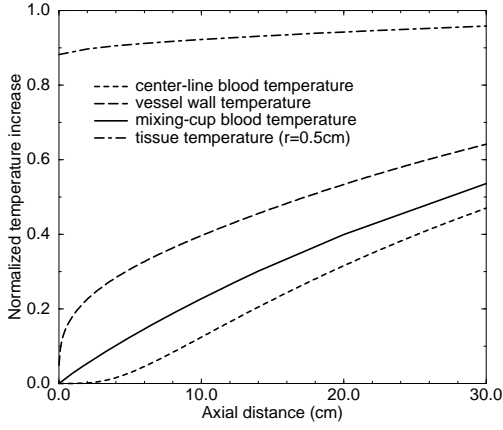|	
tissue specific heat capacity (J/g/°K):	4.180
tissue density (g/cm^3):	1.000
tissue conductivity (W/cm/°K):	0.006
blood specific heat capacity (J/g/°C):	0.006
blood density (g/cm^3):	1.000
perfusion rate (g/cm^3/s):	variable

FIGURE 3: Comparison of center-line, vessel wall and mixing-cup blood temperature of a (δ=1.4 mm) blood vessel embedded in heated tissue (w_b=0.008 g/cm³/s).

duces with increased perfusion. For example, a vessel of δ=1 mm ($<$u$>$=8cm/s), the TEL of the center-line temperature reduces from 32 cm for no perfusion to 15 cm for a perfusion of w_b= 0.008 g/cm³/s. Microvascular cooling reduces the maximum temperatures in the field and shapes the temperature profile according to the volumetric power deposition patterns. The change in the radial profiles as a function of perfusion for the BHTE is shown in figure 4a.

When microvascular cooling is modeled as an effective conductivity, similar effects are observed. Increased perfusion (k_{eff}) results in a reduction of the thermal equilibration lengths for the large vessels. For the δ=1 mm vessel, the center-line TEL reduces from 32 cm to 9.6 cm for a k_{eff} of 0.04 W/cm/°K. Furthermore, the vessel walls are at high temperatures due to the reduced thermal resistance of the surrounding tissue (Crezee and Lagendijk 1992). This shown in figure 4b. Direct comparison of the data for the two models requires a functional relationship between the effective conductivity and volumetric perfusion of tissue.

Crezee and Lagendijk (1990), in experiments in fixed bovine kidneys, provided an expression that relates effective conductivity and volumetric perfusion based on analysis of the delay and relaxation times of transient temperatures near a heat source. Assuming a linear relationship for volumetric perfusion and effective conductivity, they found:

$$k_{\mathrm{eff}} = k_{\mathrm{t}}\left(1 + \alpha w_{\mathrm{b}}\right) \qquad (3)$$

where $\alpha = 0.12$ ml/100g/min^{-1}. This relationship was utilized to compare the profiles of figures 4a and 4b. The radial temperature profiles differ for the two models; the ETCE predicts higher temperatures near the vessel
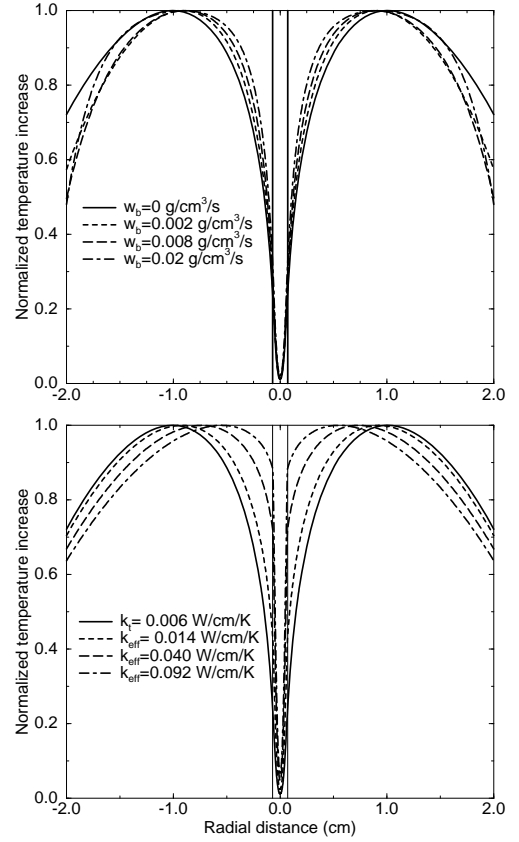

FIGURE 4: Simulated radial temperature profiles near large vessels: effect of perfusion according to the *(a)* BHTE and *(b)* ETCE model. Profiles normalized to maximum temperature at z=4 cm for a δ = 1.4mm vessel ($<$u$>$=10.5cm/s). Similar line styles in graphs correspond to equivalent effects according to equation 3.

wall. For perfusions of 0.02 g/cm³/s, the vessel wall temperature according to the BHTE is as at $\sim$35% of the maximum tissue temperature, while for the ETCE $\sim$88%. While the BHTE predicts a shortening of the TEL and higher temperatures near the large vessel for increased perfusions, the results are comparable to the ETCE model only for low tissue perfusions.

The reduction of the TEL and the increased vessel wall temperatures for the ETCE is due to the drop in thermal resistance between the vessel and the surrounding tissue (Crezee and Lagendijk 1992). In the case of the BHTE, similar reductions are due to the nature of tissue cooling: for high perfusions, the temperature distribution shapes to the power deposition pattern resulting in steeper temperature gradients closer to the large vessel and greater heat transfer. Ultimately, the theoretical models need to be validated in an experimental system.
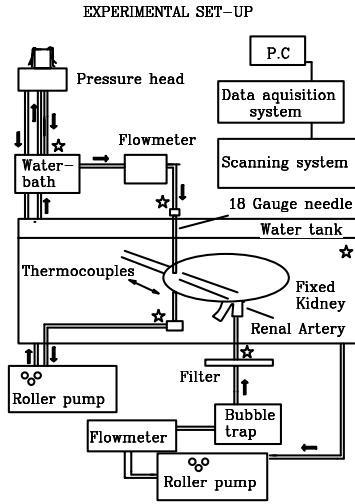
FIGURE 5: The experimental set-up consists of four main components: two *perfusion* circuits (for the phantom and the heat source), a *scanning* system and a *thermometry* data acquisition system. Thermocouples are scanned in steps of 100μm, and asterisks represent locations where temperature is measured.

Experimental results

The experiments are designed to examine temperature gradients near sources or sinks of heat and their perfusion dependence, and are similar to the experiments described by Crezee and Lagendijk (1990). The set up (figure 5) consists of a fixed porcine kidney phantom (Holmes *et al.* 1984) perfused by a peristaltic pump, an 18 Gauge hot water needle source traversing the kidney cortex, a scanning system (Hurst magnet rotor SLS-4014-002 model, Princeton, Indiana), that increments 50 μm diameter type K thermocouples in steps of 0.1 mm ($\pm 5\%$ per step) and a thermometry data acquisition system ($\pm 0.1°$C, Brown *et al.* 1992). The dynamic phantom is immersed in a waterbath kept at room temperature. Details of the experimental set-up can be found elsewhere (Kolios 1994). The radial temperature profiles created by the source are recorded and their perfusion dependence examined. Figure 6 illustrates the steady state temperature profiles obtained in the absence of kidney perfusion. The experimental data match the theoretical predictions fairly well (a logarithmic temperature profile for a simple cylindrical conduction problem). Upon perfusion, thermally significant vessels create regions of localized cooling (figure 7). X-ray angiography examination revealed a $\delta=0.6$ mm vessel close to the source in the region of the excess cooling (figure 8). This is a striking example of localized discrete vessel cooling:
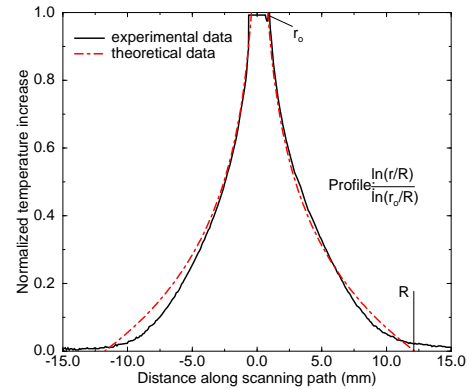

FIGURE 6: Experimental values vs. theory in the absence of perfusion. Logarithmic temperature profile indicates good agreement.

temperature gradients of 6°C/mm are observed close to the thermally significant blood vessel. Continuum models of heat transfer could not predict this temperature profile.

To compare the experimental data with the simulation results, the effects of the vessel on the temperature profile must be isolated from the temperature gradients of the heat source. Assuming that

1. the logarithmic normalized temperature profile created by the the source is not significantly altered by perfusion (which should hold if perfusion acts as an effective conductivity (Crezee and Lagendijk 1990) or for low perfusion values)

2. the presence of the vessel does not significantly alter the maximum temperature achieved in the heated field

then the normalized temperature curves for the cases of the perfused and non perfused kidneys can be subtracted to isolate the individual vessel effects. In the absence of the thermally significant vessel the subtracted profile should be a straight line along the radial axis. The temperature profiles normalized to the maximum temperatures in the field are compared in figure 9. Theoretical data are obtained for depths of 2 and 3 cm. These values were chosen by assuming the heated field in the kidney to radially extend symmetrically about the source according to the logarithmic temperature profile. The velocity of the the blood was assigned values encountered *in vivo* for a vessel of $\delta=0.6$ mm diameter ($<$u$>\sim$ 6cm/s). Despite the uncertainty in the input simulation data and experimental parameters the curves display similar trends This illustrates the ability of the model to calculate temperatures near large vessels. The analysis of the perfusion dependence of thermal gradi-
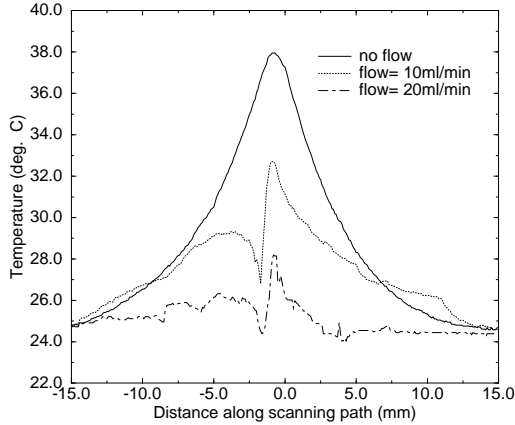
FIGURE 7: Radial temperature profiles in the presence of a thermally significant vessel (estimated $\delta \sim 0.6$ mm).

FIGURE 8: Orthogonal x-ray angiography views of the kidney phantom. Note the presence of a thermally significant vessel close to the source (at the top of the figure).

ents in tissue near sources or sinks of heat is still in progress.

Conclusions

Temperature gradients caused by thermally significant vessels can extending at least 1-2 mm from the vessel and cool adjacent tissue. Improved vascular models have been introduced to implicitly incorporate of the effects of thermal entrance regions, local heating, vessel shape and transient temperature gradients on heat transfer to large vessels. Parametric studies demonstrated that perfused tissues, modeled either as a heat sink or an effective conductivity, have the ability to reduce the TEL and increase tissue and vessel wall temperatures of large vessels. Direct comparison illustrates that microvascular heat transfer according to the ETCE is more effective in vessel heating than the BHTE for equivalent volumetric
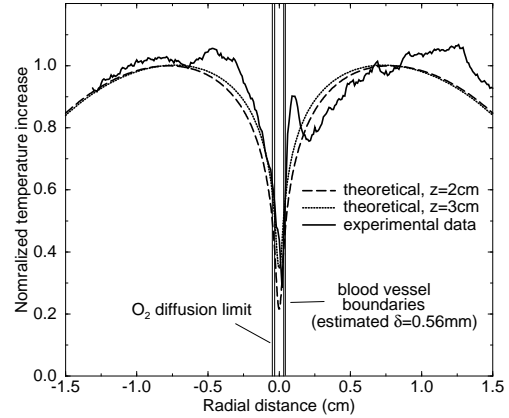

FIGURE 9: Simulations and experimental data. Although modeling different situations, a general agreement in the profiles is seen. Simulation data for depths of 2, 3cm for a $\delta = 0.6$ mm vessel with a velocity of 6cm/s (w_b=0.002gr/cm^3/s, BHTE).

perfusion values, resulting in shorter TELs and higher tissue temperatures near the vessel. High spatial resolution experiments indicate that vessels of diameter $\sim$ 0.6 mm can induce temperature gradients of 6°C/mm in heated regions. Comparison of the theoretical simulations and the experimental data, albeit modeling different situations, shown a general agreement in predictions of temperature profiles. The data also illustrate the importance of high temperature spatial resolution for the interpretation of *in vivo* temperature profiles; scanning steps of 1 mm, typical for bioheat transfer experiments, can miss significant vessel information and potentially lead to erroneous interpretation of profiles. This is clearly seen in figure 7. Provided that blood vessel geometry and flow information can be obtained by an imaging modality and accurate models of microvascular bioheat transfer are utilized, thermal modeling should provide accurate temperature profiles of heated tissues.
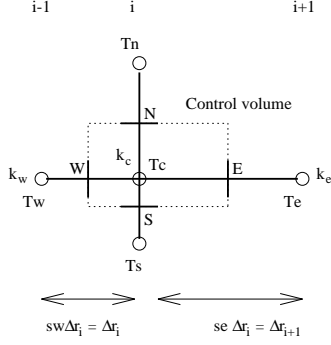
Acknowledgments

FIGURE 10: Finite difference representation of nodes.

Appendix

The finite difference approximations to the derivatives of the bioheat equation are derived for nodes with variable conductivity and uneven spacing in the radial direction. Following the notation of figure 10, the derivative at point c can be calculated by taking the weighted average of the two one-sided derivatives between nodes (w and c) and (c and e), which define a control volume. The approximation to the first derivative is becomes:

$$k\frac{dT}{dr}\big|_c = \frac{s_e}{s_e + s_w}\frac{dT}{dr}\big|_{r=W} kW + \frac{s_w}{s_e + s_w}\frac{dT}{dr}\big|_{r=E} kE \quad (4)$$

Assume that nodes e and c have a conductivity k_e, and that node w has a conductivity of k_w. The conductivities kE and kW can be approximated by kE=k_e and $kW = (k_e k_w)/k_e k_w = k_h$, where k_h is the harmonic mean of k_e and k_w (Patankar 1980). Assuming a piecewise linear profile for the temperature variation in between the nodes of the grid, 4 becomes:

$$k\frac{dT}{dr} = \frac{s_e}{s_e + s_w}\frac{T_c - T_w}{s_w \, dr} k_h + \frac{s_w}{s_e + s_w}\frac{T_e - T_c}{s_e \, dr} k_e \quad (5)$$

Note that for $k_e = k_h$ and $s_w=s_e=1$, the derivative is equivalent to the central difference formulae. The second derivative can be calculated in a similar fashion and is given by the difference of the two one-sided derivatives, estimated at W and E, divided by their distance.

Differentials in the axial direction were discretized according to central differences for conductive gradients and upwind differencing for convective gradients. The expressions were substituted in equations (1 and 2). To solve the algebraic problem, the Alternate Direction Implicit method was used. The algorithm separates each timestep into two parts, for which it solves one coordinate direction implicitly in the first part and the other coordinate direction implicitly for the second part. The time discretization is split into two steps. In the first step, the time derivative is replaced by $\frac{dT}{dt} = \frac{2(T_c^{1/2} - T_c)}{dt}$,

while in the second step by $\frac{dT}{dt} = \frac{2(T_c^1 - T_c^{1/2})}{dt}$. Upon substitution and solving for the r-direction implicitly and the unknowns $T_c^{1/2}, T_w^{1/2}, T_e^{1/2}$ (letting $r = idr_i$):

$$\left(\left(\left(\frac{s_e k_h}{(s_e + s_w) s_w} - \frac{s_w k_e}{(s_e + s_w) s_e}\right) i^{-1}\right.\right.$$
$$+ \left(-\frac{2 k_e}{s_e} - \frac{2 k_h}{s_w}\right)(s_e + s_w)^{-1}\right) dr_i^{-2} - \frac{r_b c_b}{2 \, dt}\right) T_c^{1/2}$$
$$+ \left(\frac{2 k_h}{(s_e + s_w) s_w} - \frac{s_e k_h}{i \,(s_e + s_w) s_w}\right) T_w^{1/2} dr_i^{-2}$$
$$+ \left(\frac{2 k_e}{(s_e + s_w) s_e} + \frac{s_w k_e}{i \,(s_e + s_w) s_e}\right) T_e^{1/2} dr_i^{-2} =$$
$$-\frac{r_b c_b T_c}{2 \, dt} + w_b c_b \,(T_c - T_{art}) - Q +$$
$$\frac{r_b c_b u_b \,(T_s - T_c)}{dz} - \frac{T_n - 2 T_c + T_s}{dz^2}$$
$$(6)$$

The terms on the right hand side of the equation and all the terms in the parenthesis are known. A system of n equations with n unknowns results when the above expressions are written for each node in the solution domain. The second and final step calculates the solution for T_c^1, T_n^1 and T_s^1. Repeating the above procedure and solving for z implicitly results in a similar expression. Note that three unknowns result from each equation, and thus if the equations are written in matrix format, the solution matrix will be tri-diagonal, simplifying and accelerating the solution procedure (Ames, 1979).

To generate a uniform grid, each coordinate location is represented by r(i)=idr where i is an integer. In this work dr is varied. Assume each coordinate location is given by r(i)=iΔ_i, where Δ_i= f(i). In this case, the spacing between two locations on the grid is a function of i and is given by

$$dr_i = i\Delta_i - (i-1)\Delta_{i-1} \text{ for } i > 0, \quad (7)$$

The function Δ_i determines the grid spacing. A linear increase in grid spacing was used, concentrating points near the blood vessel. To linearly increase the grid spacing, Δ_i was defined as:

$$\Delta_i \equiv \Delta_{min} + i\Delta_{inc} \quad (8)$$

where Δ_{min} determines the minimum node spacing and Δ_{inc} a parameter that determines the rate of change of node spacing. According to the above, the node spacing is

$$dr_i \equiv i\Delta_i - (i-1)\Delta_{i-1} = \Delta_{min} + (2i-1)\Delta_{inc} \quad (9)$$

for $i > 0$, increasing linearly with i. Note that Δ_i can be defined as any function of i, and thus other grid spacings can be derived by defining Δ_i accordingly (as a sinusoid for example). In this work, for each node i, dr_i and dr_{i+1} were calculated using the above equations. The parameters Δ_{inc} and Δ_{min} were set to 1.6 10^{-5}mm and 2.0 10^{-5}mm respectively and i typically varied from 0 to 600. The axial spacing was dz=1mm. The parameter sw was set to 1 and thus dr_i was used as the reference node spacing in figure 10. Hence, $se= \frac{dr_{i+1}}{dr_i}$. Utilizing the finite difference relationships derived in this appendix and spacings according to the above, the system was solved, giving a unique solution for each node (Kolios 1994).

References

Baish, J. (1992). Formulation of a statistical model of heat transfer in perfused tissue. In *ASME Advances in Biological Heat and Mass Transfer -1992-*, Winter Annual Meeting, pp. 135–140. American Society of Mechanical Engineers.

Basmadjian, D. (1990). The effect of flow and mass transport in thrombogenesis. *Annals of Biomedical Engineering 18*, 685–709.

Brown, S., X. Li, H. Pai, R. Hill, and J. Hunt (1992). Observations of thermal gradients in perfused tissues using water bath heating. *International Journal of Hyperthermia 8*(2), 275–287.

Chen, Z. and R. Roemer (1992). The effects of large blood vessels on temperature distributions during hyperthermia. *Journal of Biomechanical Engineering 114*, 473–481.

Crezee, J. and J. Lagendijk (1990). Experimental verification of bio-heat transfer thoeries: measurement of temperature profiles around large artificial vessels in perfused tissue. *Physics in Medicine and Biology 35*(7), 905–923.

Crezee, J. and J. Lagendijk (1992). Temperature uniformity during hyperthermia: the impact of large vessels. *Physics in Medicine and Biology 37*(6), 1321–1337.

Crezee, J., J. Mooibroek, C. Bos, and J. Lagnedijk (1991). Interstitial heating: experiments in artificially perfused bovine tongues. *Physics in Medicine and Biology 36*(6), 823–833.

Croft, D. and D. Lilley (1977). *Heat transfer calculations using finite difference equations*. Essex: Applied Science Publishers Ltd.

Duck, F. (1990). *Physical Properties of Tissues: A Comprehensive Reference Book*. San Diego: Academic Press.

Holmes, K., W. Ryan, P. Wienstein, and M. Chen (1984). A fixation technique for organs to be used as perfused tissue phantoms in bioheat transfer studies. *ASME Advances in Bioengineering*, 9–10.

Kolios, M. (1994). Models of bioheat transfer during hyperthermia. Master's thesis, University of Toronto.

Lagendijk, J., J. Crezee, and J. Mooibroek (1992). Progess in thermal modeling developement. In E. Gerner and T. Cetas (Eds.), *Proceedings of the 6th International Congress on Hyperthermic Oncology*, Volume 2 of *Hyperthermic Oncology 1992*, pp. 257–261. Taylor and Francis.

Mooibroek, J. and J. Langendijk (1991). A fast and simple algorithm for the calculation of convective heat transfer by large vessels in three-dimnesional inhomogeneous tissues. *IEEE Transactions in Biomedical Engineering 38*(5), 490–501.

Moros, E., A. Dutton, R. Roemer, M. Burton, and K. Hynynen (1993a). Experimental evaluation of two simple thermal models using hyperthermia in vivo. *International Journal of Hyperthermia 9*(4), 581–598.

Moros, E., W. Straube, and R. Myerson (1993b). Finite difference vascular model for 3-d cancer therapy with hyperthermia. In R. Roemer (Ed.), *Advances in Biological and Heat and Mass Transfer*, Volume HTD-268, pp. 107–111. ASME, Heat Transfer Division.

Patankar, S. (1980). *Numerical heat transfer and fluid flow*. Washington, D.C.: Hemisphere.

Roemer, R. (1990). The local tissue cooling coefficient: a unified approach to thermal washout and steady-state 'perfusion' calculations. *International Journal of Hyperthermia 6*(2), 421–430.

Sapareto, S. and W. Dewey (1984). Thermal dose determination in cancer therapy. *International Journal of Radiation Oncology, Biology and Physics 10*, 787–800.

Shah, R. and A. London (1978). *Laminar flow forced convection in ducts*. Academic Press.

Soliman, M. and P. Chambre (1967). On the time dependent leveque problem. *International Journal of Heat and Mass Transfer 10*, 169–180.